

RUNNs: Ritz–Uzawa Neural Networks for Solving Variational Problems

Pablo Herrera^{1,4}, Jamie M. Taylor⁷, Carlos Uriarte^{1,2}, Ignacio Muga⁴, David Pardo^{3,1,6}, and
Kristoffer G. van der Zee⁵

¹Basque Center for Applied Mathematics, Bilbao, Spain

²Curtin University, Perth, Australia

³Department of Mathematics, University of the Basque Country UPV/EHU, Leioa, Spain

⁴Instituto de Matemáticas, Pontificia Universidad Católica de Valparaíso, Valparaíso, Chile

⁵School of Mathematical Sciences, University of Nottingham, Nottingham, UK

⁶Ikerbasque: Basque Foundation for Science, Bilbao, Spain

⁷Department of Mathematics, CUNEF Universidad, Madrid, Spain

March 16, 2026

Abstract

Solving Partial Differential Equations (PDEs) using neural networks presents different challenges, including integration errors and spectral bias, often leading to poor approximations. In addition, standard neural network-based methods, such as Physics-Informed Neural Networks (PINNs), often lack stability when dealing with PDEs characterized by low-regularity solutions.

To address these limitations, we introduce the Ritz–Uzawa Neural Networks (RUNNs) framework, an iterative methodology to solve strong, weak, and ultra-weak variational formulations. Rewriting the PDE as a sequence of Ritz-type minimization problems within a Uzawa loop provides an iterative framework that, in specific cases, reduces both bias and variance during training. We demonstrate that the strong formulation offers a passive variance reduction mechanism, whereas variance remains persistent in weak and ultra-weak regimes. Furthermore, we address the spectral bias of standard architectures through a data-driven frequency tuning strategy. By initializing a Sinusoidal Fourier Feature Mapping based on the Normalized Cumulative Power Spectral Density (NCPSD) of previous residuals or their proxies, the network dynamically adapts its bandwidth to capture high-frequency components and severe singularities. Numerical experiments demonstrate the robustness of RUNNs, accurately resolving highly oscillatory solutions and successfully recovering a discontinuous L^2 solution from a distributional H^{-2} source—a scenario where standard energy-based methods fail.

Keywords: Physics-Informed Neural Networks; Deep Ritz Method; Inexact Uzawa Method; Saddle-point problems; Spectral bias; Numerical integration; Variational formulations.

1 Introduction

Neural Networks (NNs) have become a useful tool for solving Partial Differential Equations (PDEs), providing a way to solve high-dimensional or parametric problems by transforming the PDE into a minimization problem via a loss function [12, 18]. Specifically, developing robust, mesh-free solvers for differential equations allows for the accurate simulation of physical phenomena in engineering and science, avoiding the limitations of traditional mesh generation (i.e., curse of dimensionality).

Common examples of this approach include Physics-Informed Neural Networks (PINNs) [18], which minimize the strong form of the residual, and the Deep Ritz Method (DRM) [12], which minimizes the energy functional associated with the variational form. Despite their use, practical challenges remain. First, there is often a mismatch between the regularity of the exact solution and the space spanned by the neural network, especially in problems with low-regularity solutions where standard PINNs may fail. Second, approximating the loss function

via quadrature rules introduces bias and variance. As shown in [19, 24], these integration errors can prevent the network from finding the true minimizer, leading to overfitting even with an ideal optimization path.

To address the stability issues of pure minimization, some approaches use dual norms. For instance, Robust Variational PINNs (RVPINNs) [20] and Machine-Learning Minimal-Residual (ML-MRes) frameworks [7] minimize residuals in dual norms. Similarly, using the classical resolution of saddle-point problems [3, 27], recent works have proposed neural implementations of the Uzawa iteration. These include Deep Uzawa [16] and the Inexact Uzawa-Double Deep Ritz method [4], which replace trial and test spaces with neural networks. While these methods improve stability, they typically overlook the spectral bias inherent in standard architectures and do not explicitly address the relationship between the iterative scheme and the reduction of integration variance in data-scarce regimes.

Our main contribution in this paper is the proposal of the Ritz–Uzawa Neural Networks (RUNNs) framework to iteratively solve linear PDEs in strong, weak, and ultra-weak variational formulations. The RUNNs framework reformulates the PDE as a sequence of Ritz-type minimizations inside a Uzawa loop; for strong formulations, this approach inherently reduces both integration bias and variance. This framework is based on the Inexact Uzawa Method [6], which preserves convergence even when inner sub-problems are solved approximately. Furthermore, we explicitly address the spectral bias of neural networks [22, 23, 28] by employing Sinusoidal Fourier Feature Mapping to approximate dual variables, allowing efficient capture of high-frequency error components through iterative corrections.

The methodology approximates the primal and dual variables with neural networks trained via a hybrid optimization strategy combining Least Squares and Adam (LS/Adam) [11, 15, 25]. This combination handles linear and non-linear parameters efficiently. We demonstrate that RUNNs show better stability compared to the standard Deep Ritz Method, particularly when dealing with solutions of low regularity (e.g., solutions in L^2 that do not belong to H_0^1) and high frequency behavior.

The paper is organized as follows. Section 2 establishes the abstract mathematical framework and proves the convergence of the inexact Uzawa method, categorizing the resolution into three distinct optimization approaches (Approaches 1, 2, and 3). Specifically, it extends the iterative scheme to solve strong, weak, and ultra-weak variational formulations, analyzing the contraction properties of the involved operator and demonstrating how these formulations generalize existing methods like the Deep Double Ritz Method (D²RM) and multilevel neural networks. Section 3 describes the neural network architectures employed, introducing a hybrid model that combines standard Multilayer Perceptrons (MLPs) with a Sinusoidal Fourier Feature Mapping. This section details an adaptive strategy that uses the Normalized Cumulative Power Spectral Density (NCPSD) of the residuals to tune the frequency bandwidth, effectively mitigating spectral bias. Furthermore, it presents the hybrid Least Squares/Adam (LS/Adam) optimization strategy, which decouples the training of linear and non-linear parameters using Tikhonov regularization for the output layer. Section 4 discusses the discretization of the loss function, implementing third-order unbiased stratified stochastic quadrature rules to control integration bias. It also provides a theoretical analysis of the bias-variance asymptotics, highlighting the difference in passive variance reduction between strong formulations (where variance tends to zero) and variational formulations (where variance remains non-zero). Finally, Section 5 presents numerical experiments validating the approach. These include a comparison of convergence rates between pure Adam and LS/Adam, a high-frequency problem (40π) solved via spectral matching, and a challenging test case for an ultra-weak formulation with a distributional H^{-2} source term (the derivative of a Dirac delta), where the method successfully recovers a discontinuous solution in L^2 that falls outside the standard H_0^1 space.

2 Mathematical Framework

2.1 Model problem

Let \mathbb{U} and \mathbb{V} be two Hilbert spaces endowed with inner products $(\cdot, \cdot)_{\mathbb{U}}$ and $(\cdot, \cdot)_{\mathbb{V}}$, respectively. Let $b : \mathbb{U} \times \mathbb{V} \rightarrow \mathbb{R}$ be a bilinear form, such that for any given continuous linear functional $\ell : \mathbb{V} \rightarrow \mathbb{R}$, the following variational problem admits a unique solution:

$$\begin{cases} \text{Find } u^* \in \mathbb{U} \text{ such that} \\ b(u^*, v) = \ell(v), \forall v \in \mathbb{V}. \end{cases} \quad (1)$$

It is well-known (see, e.g., [13, Theorem 25.9]) that problem (1) admits a unique solution whenever the following conditions hold:

$$\mathbf{Continuity:} \quad \exists M > 0 \text{ such that } |b(u, v)| \leq M \|u\|_{\mathbb{U}} \|v\|_{\mathbb{V}}, \quad \forall u \in \mathbb{U} \text{ and } \forall v \in \mathbb{V}. \quad (2)$$

$$\mathbf{Injectivity:} \quad \exists \gamma_1 > 0 \text{ such that } \sup_{v \in \mathbb{V} \setminus \{0\}} \frac{|b(u, v)|}{\|v\|_{\mathbb{V}}} \geq \gamma_1 \|u\|_{\mathbb{U}}, \quad \forall u \in \mathbb{U}. \quad (3)$$

$$\mathbf{Surjectivity:} \quad \exists \gamma_2 > 0 \text{ such that } \sup_{u \in \mathbb{U} \setminus \{0\}} \frac{|b(u, v)|}{\|u\|_{\mathbb{U}}} \geq \gamma_2 \|v\|_{\mathbb{V}}, \quad \forall v \in \mathbb{V}. \quad (4)$$

As a result, these constants are equal (i.e., $\gamma_1 = \gamma_2 =: \gamma$) in the case where we take the optimal constants satisfying the requirements, and the following upper and lower bounds hold:

$$\gamma \|u\|_{\mathbb{U}} \leq \sup_{v \in \mathbb{V} \setminus \{0\}} \frac{|b(u, v)|}{\|v\|_{\mathbb{V}}} \leq M \|u\|_{\mathbb{U}}, \quad u \in \mathbb{U}. \quad (5)$$

2.2 The Uzawa method

Given $u \in \mathbb{U}$, we define the residual representative $r = r(u) \in \mathbb{V}$ as the unique solution to the following variational problem:

$$(r, v)_{\mathbb{V}} = \ell(v) - b(u, v) = b(u^* - u, v), \quad \forall v \in \mathbb{V}. \quad (6)$$

The residual r is the Riesz representative in \mathbb{V} of the functional $v \mapsto b(u^* - u, v)$.

Now, let us define $\delta = \delta(r)$ as the unique solution of the following problem:

$$(\delta, w)_{\mathbb{U}} = b(w, r), \quad \forall w \in \mathbb{U}. \quad (7)$$

Analogously, δ is the Riesz representative in \mathbb{U} of the continuous linear functional $w \mapsto b(w, r)$. Therefore, δ acts as the optimal correction direction in the trial space driven by the residual r .

Proposition 1. Let $\{u^k\} \subset \mathbb{U}$ be a sequence and define $\{r^k\} := \{r(u^k)\} \subset \mathbb{V}$ and $\{\delta^k\} = \{\delta(r^k)\} \subset \mathbb{U}$. Then, the following statements are equivalent:

- (i) $\{u^k\} \rightarrow u^*$ in \mathbb{U} .
- (ii) $\{r^k\} \rightarrow 0_{\mathbb{V}}$ in \mathbb{V} .
- (iii) $\{\delta^k\} \rightarrow 0_{\mathbb{U}}$ in \mathbb{U} .

Proof. If $\{u^k\} \rightarrow u^*$ in \mathbb{U} , then

$$\|r^k\|_{\mathbb{V}} = \sup_{v \in \mathbb{V}} \frac{(r^k, v)_{\mathbb{V}}}{\|v\|_{\mathbb{V}}} = \sup_{v \in \mathbb{V}} \frac{b(u^* - u^k, v)}{\|v\|_{\mathbb{V}}} \leq M \|u^* - u^k\|_{\mathbb{U}}, \quad (\text{by (6) and (2)})$$

which proves (i) \Rightarrow (ii). If $\{r^k\} \rightarrow 0_{\mathbb{V}}$ in \mathbb{V} , then

$$\|\delta^k\|_{\mathbb{U}} = \sup_{w \in \mathbb{U}} \frac{(\delta^k, w)_{\mathbb{U}}}{\|w\|_{\mathbb{U}}} = \sup_{w \in \mathbb{U}} \frac{b(w, r^k)}{\|w\|_{\mathbb{U}}} \leq M \|r^k\|_{\mathbb{V}}, \quad (\text{by (7) and (2)})$$

which proves (ii) \Rightarrow (iii). If $\{\delta^k\} \rightarrow 0_{\mathbb{U}}$ in \mathbb{U} , then

$$\|u^* - u^k\|_{\mathbb{U}} \leq \frac{1}{\gamma} \sup_{v \in \mathbb{V}} \frac{b(u^* - u^k, v)}{\|v\|_{\mathbb{V}}} = \frac{1}{\gamma} \|r^k\|_{\mathbb{V}} \leq \frac{1}{\gamma^2} \sup_{w \in \mathbb{U}} \frac{b(w, r^k)}{\|w\|_{\mathbb{U}}} = \frac{1}{\gamma^2} \|\delta^k\|_{\mathbb{U}}, \quad (\text{by (3), (6), (5) and (7)})$$

which proves (iii) \Rightarrow (i). \square

Given an initial guess $u^0 \in \mathbb{U}$, the Uzawa method (see e.g., [2, 4, 27]) constructs a sequence $\{u^k\} \subset \mathbb{U}$ whose elements are updated in the direction of $\delta^k = \delta(r^k) = \delta(r(u^k))$ with a step size $\rho > 0$ as follows:

$$\begin{cases} u^0 \in \mathbb{U}, \\ u^{k+1} = u^k + \rho \delta^k = u^0 + \rho \sum_{j=0}^k \delta^j. \end{cases} \quad (8)$$

The hyperparameter $\rho > 0$ is chosen to ensure the convergence of the method, as discussed below.

2.3 Convergence of the Uzawa method

Let $B : \mathbb{U} \rightarrow \mathbb{V}$ and $B' : \mathbb{V} \rightarrow \mathbb{U}$ be the trial-to-test and test-to-trial operators inherited from the bilinear form $b(\cdot, \cdot)$ as follows:

$$(Bu, v)_{\mathbb{V}} = b(u, v) = (u, B'v)_{\mathbb{U}}, \quad u \in \mathbb{U}, v \in \mathbb{V}. \quad (9)$$

Then,

$$r^k = B(u^* - u^k) \quad \text{and} \quad \delta^k = B'r^k = B'B(u^* - u^k).$$

Defining the error $e^k := u^* - u^k$, the iterative scheme (8) yields

$$e^{k+1} = u^* - u^{k+1} = u^* - u^k - \rho\delta^k = (I - \rho B'B)(u^* - u^k) = (I - \rho B'B)e^k. \quad (10)$$

Proposition 2. The operator $I - \rho B'B$ is a contraction (hence, $\{u^k\} \rightarrow u^*$) whenever $\rho < 2\|B\|^{-2}$. Indeed, the optimal choice for ρ is $\rho^* := 2/(\|B\|^2 + \|B^{-1}\|^{-2})$, with optimal contraction rate given by

$$\|I - \rho^* B'B\| = \frac{\|B\|^2 - \|B^{-1}\|^{-2}}{\|B\|^2 + \|B^{-1}\|^{-2}}.$$

Proof. Because $B'B$ is self-adjoint, so is $I - \rho B'B$. Using [8, Proposition 6.9], we have that $\|I - \rho B'B\| < 1$ is satisfied provided

$$-\|u\|_{\mathbb{U}}^2 < \|u\|_{\mathbb{U}}^2 - \rho\|Bu\|_{\mathbb{V}}^2 < \|u\|_{\mathbb{U}}^2, \quad \forall u \in \mathbb{U} \setminus \{0_{\mathbb{U}}\}.$$

The upper bound is always satisfied because $\rho > 0$, while the lower bound is satisfied when

$$\rho < 2 \left(\frac{\|u\|_{\mathbb{U}}}{\|Bu\|_{\mathbb{V}}} \right)^2, \quad \forall u \in \mathbb{U} \setminus \{0_{\mathbb{U}}\}.$$

The upper bound is minimized when $\|Bu\|_{\mathbb{V}}/\|u\|_{\mathbb{U}}$ attains its maximum value, yielding $\rho \leq 2\|B\|^{-2}$. Moreover,

$$\begin{aligned} \|I - \rho B'B\| &= \max_{u \neq 0} \left| 1 - \rho \frac{\|Bu\|_{\mathbb{V}}^2}{\|u\|_{\mathbb{U}}^2} \right| = \max \left\{ \rho\|B\|^2 - 1, 1 - \rho/\|B^{-1}\|^2 \right\} \\ &= \begin{cases} \rho\|B\|^2 - 1 & \text{if } \rho \geq 2(\|B^{-1}\|^{-2} + \|B\|^2)^{-1}; \\ 1 - \rho/\|B^{-1}\|^2 & \text{if } \rho \leq 2(\|B^{-1}\|^{-2} + \|B\|^2)^{-1}, \end{cases} \end{aligned}$$

whose minimum (as a function of ρ), is attained exactly at $\rho^* = 2(\|B^{-1}\|^{-2} + \|B\|^2)^{-1}$. \square

Remark 1 (Ideal convergence with graph inner product). By equipping \mathbb{U} with the graph inner product $(u, w)_{\mathbb{U}} := (Bu, Bw)_{\mathbb{V}}$, we obtain $B' = B^{-1}$. As a result,

$$e^{k+1} = (1 - \rho)e^k, \quad (11)$$

which yields the optimal choice $\rho^* = 1$ that reduces the iterative scheme to a single step.

2.4 Combining Ritz and Uzawa: three approaches

Following the definitions of (6) and (7), for an initial guess $u^0 \in \mathbb{U}$, the Uzawa iterative method reads as:

$$\begin{cases} (r^k, v)_{\mathbb{V}} = \ell(v) - b(u^k, v), \quad \forall v \in \mathbb{V}; \\ (\delta^k, w)_{\mathbb{U}} = b(w, r^k), \quad \forall w \in \mathbb{U}; \\ u^{k+1} = u^k + \rho\delta^k. \end{cases} \quad (12)$$

Now, to address the variational characterizations of r^k and δ^k , we reformulate them as optimization problems in the following three ways:

2.4.1 Approach 1

We formulate the computation of the residual r^k and the correction δ^k in terms of suitable Ritz minimization problems within the continuous spaces \mathbb{V} and \mathbb{U} , respectively. We then construct the updated solution u^{k+1} following the summation scheme indicated in (8), which yields the following exact iterative method:

$$\begin{cases} r^k &= \arg \min_{r \in \mathbb{V}} \frac{1}{2} \|r\|_{\mathbb{V}}^2 - \ell(r) + b(u^k, r) \\ \delta^k &= \arg \min_{\delta \in \mathbb{U}} \frac{1}{2} \|\delta\|_{\mathbb{U}}^2 - b(\delta, r^k) \\ u^{k+1} &= u^0 + \rho\delta^0 + \rho\delta^1 + \dots + \rho\delta^k. \end{cases} \quad (13)$$

Notice that (13) can be viewed as a generalization of the work on multilevel neural networks developed in [1] to (variational) problems using the Ritz method. We emphasize that this approach does not require the bilinear form b to be symmetric.

2.4.2 Approach 2

The function spaces defined by neural network architectures are generally not closed under addition. This implies that explicitly computing and storing the sum that defines u^{k+1} in Approach 1 could become prohibitively expensive in memory as the iteration count k increases. To avoid this limitation, we reformulate the update step as an additional optimization problem within the continuous setting. Specifically, we replace the summation with the following \mathbb{U} -norm minimization problem:

$$u^{k+1} = \arg \min_{u \in \mathbb{U}} \|u - (u^k + \rho\delta^k)\|_{\mathbb{U}}^2. \quad (14)$$

By framing the update as a projection, the exact method reads as follows:

$$\begin{cases} \text{Given } u^0 \in \mathbb{U}, \text{ let} \\ r^k = \arg \min_{r \in \mathbb{V}} \frac{1}{2} \|r\|_{\mathbb{V}}^2 - \ell(r) + b(u^k, r); \\ \delta^k = \arg \min_{\delta \in \mathbb{U}} \frac{1}{2} \|\delta\|_{\mathbb{U}}^2 - b(\delta, r^k); \\ u^{k+1} = \arg \min_{u \in \mathbb{U}} \|u - (u^k + \rho\delta^k)\|_{\mathbb{U}}^2. \end{cases} \quad (15)$$

As with Approach 1, this continuous formulation has the advantage that the integrands of the loss functions associated with r^k and δ^k tend to zero at convergence. Furthermore, defining u^{k+1} via minimization avoids the need to dynamically expand the network architecture during the iterative process.

2.4.3 Approach 3

Replacing δ^k with $\frac{u^{k+1} - u^k}{\rho}$ in (12), simplifying u^{k+1} and rewriting the resulting equation as a minimization problem, we obtain the following two-step minimization scheme:

$$\begin{cases} r^k &= \arg \min_{r \in \mathbb{V}} \frac{1}{2} \|r\|_{\mathbb{V}}^2 - \ell(r) + b(u^k, r), \\ u^{k+1} &= \arg \min_{u \in \mathbb{U}} \frac{1}{2} \|u\|_{\mathbb{U}}^2 - (u^k, u)_{\mathbb{U}} - \rho b(u, r^k). \end{cases} \quad (16)$$

The integrand of the second minimization does not converge to zero during the iterative process. In Section 2.5, we show how this approach relates to the DRM, the Deep Double Ritz Method (D²RM), and the Adjoint Ritz minimization with post-processing [12, 26].

2.5 Simplifications under Different Problem Formulations

2.5.1 Strong Formulation

In a strong formulation, we propose the following framework.

- $B : \mathbb{U} \rightarrow L^2$ is the PDE operator and $f \in L^2$ is the source.
- $b(u, v) = (Bu, v)_{L^2}$ is the bilinear form and $\ell(v) = (f, v)_{L^2}$ is the right-hand side for all $u \in \mathbb{U}$ and all $v \in L^2$. Recalling Remark 1, by equipping \mathbb{U} with the graph inner product $(u, w)_{\mathbb{U}} := (Bu, Bw)_{L^2}$, we have that $\rho^* = 1$ is an optimal choice in Uzawa.
- The Ritz minimization for r^k is unnecessary, as r^k is explicitly available: $r^k = f - Bu^k$.
- The resulting variational problem on δ^k ,

$$\underbrace{(\delta^k, w)_{\mathbb{U}}}_{(B\delta^k, Bw)_{L^2}} = \underbrace{b(w, r^k)}_{(Bw, f - Bu^k)_{L^2}}, \quad \forall w \in \mathbb{U},$$

can be reformulated, since B is surjective onto L^2 , as the following L^2 -norm minimization problem:

$$\delta^k = \arg \min_{\delta \in \mathbb{U}} \|B\delta + Bu^k - f\|_{L^2}^2.$$

As a result, Approaches 1-3 simplify as follows:

Approach 1 (S). Given u^k , we have:

$$\begin{cases} \delta^k &= \arg \min_{\delta \in \mathbb{U}} \|B\delta + Bu^k - f\|_{L^2}^2 \\ u^{k+1} &= u^0 + \delta^0 + \delta^1 + \dots + \delta^k. \end{cases} \quad (17)$$

In particular, this iterative method is referred to as the multilevel neural network method in [1].

Approach 2 (S). Given u^k , we have:

$$\begin{cases} \delta^k &= \arg \min_{\delta \in \mathbb{U}} \|B\delta + Bu^k - f\|_{L^2}^2 \\ u^{k+1} &= \arg \min_{u \in \mathbb{U}} \|B\delta^k + Bu^k - Bu\|_{L^2}^2. \end{cases} \quad (18)$$

Approach 3 (S). We obtain the Deep Double Ritz method (D²RM) [26]:

$$u^{k+1} = \arg \min_{u \in \mathbb{U}} \frac{1}{2} \|Bu\|_{L^2}^2 - (f, Bu)_{L^2}. \quad (19)$$

2.5.2 Weak formulation

In symmetric and positive-definite problems, we propose the following framework:

- $\mathbb{U} = \mathbb{V}$ are equipped with the inner product driven by the bilinear form $b(\cdot, \cdot)$. Thus, B is the identity operator, and \mathbb{U} can be read as equipped with the graph inner product (recall Remark 1). Then, $\rho^* = 1$.
- We have $\mathbb{V} \ni r^k = \delta^k = u^* - u^k \in \mathbb{U}$. Then, we can remove the formulations related to δ^k and directly consider $u^{k+1} = u^k + r^k$.

As a result, Approaches 1-3 simplify as follows:

Approach 1 (W). Given u^k , we have:

$$\begin{cases} r^k &= \arg \min_{r \in \mathbb{V}} \frac{1}{2} b(r, r) + b(u^k, r) - \ell(r), \\ u^{k+1} &= u^0 + r^0 + r^1 + \dots + r^k. \end{cases} \quad (20)$$

Approach 2 (W). Given u^k , we have:

$$\begin{cases} r^k &= \arg \min_{r \in \mathbb{V}} \frac{1}{2} b(r, r) + b(u^k, r) - \ell(r), \\ u^{k+1} &= \arg \min_{u \in \mathbb{U}} b(r^k + u^k - u, r^k + u^k - u). \end{cases} \quad (21)$$

Approach 3 (W). We recover the traditional Ritz minimization.

$$u^{k+1} = \arg \min_{u \in \mathbb{U}} \frac{1}{2} b(u, u) - \ell(u). \quad (22)$$

2.5.3 Ultra-weak formulation

In ultra-weak formulations, $\mathbb{U} = L^2$, $b(u, v) = (u, B'v)_{L^2}$ and $\ell(v) = (f, v)_{L^2}$ for all $u \in L^2$ and all $v \in \mathbb{V}$. Under this framework, the following properties hold:

- By equipping \mathbb{V} with the inner product $(\cdot, \cdot)_{\mathbb{V}} := (B'\cdot, B'\cdot)_{L^2}$, we obtain $\rho^* = 1$ as the optimal step size (recall Remark 1).
- The Ritz minimization for δ^k is explicitly available as $\delta^k = B'r^k$, thus avoiding the need to compute it numerically.

As a result, Approaches 1-3 simplify as follows:

Approach 1 (U). Given u^k :

$$\begin{cases} r^k &= \arg \min_{r \in \mathbb{V}} \frac{1}{2} (B'r, B'r)_{L^2} + b(u^k, r) - \ell(r), \\ u^{k+1} &= u^0 + B'r^0 + B'r^1 + \dots + B'r^k. \end{cases} \quad (23)$$

Approach 2 (U). Given u^k :

$$\begin{cases} r^k &= \arg \min_{r \in \mathbb{V}} \frac{1}{2} (B'r, B'r)_{L^2} + b(u^k, r) - \ell(r), \\ u^{k+1} &= \arg \min_{u \in \mathbb{U}} \|B'r^k + u^k - u\|_{L^2}^2. \end{cases} \quad (24)$$

Approach 3 (U). We recover the Adjoint Ritz minimization with post-processing mentioned in [26]. Given u^k :

$$\begin{cases} r &= \arg \min_{r \in \mathbb{V}} \frac{1}{2} \|B'r\|_{L^2}^2 - \ell(r), \\ u^{k+1} &= B'r. \end{cases} \quad (25)$$

2.6 Practical Setup: Inexact Uzawa Method

In practice, mainly due to the imprecision of minimization algorithms such as those used for training neural networks, the exact minimizations described in Approaches 1, 2 and 3 cannot be solved perfectly. Optimization algorithms introduce approximation errors, meaning we only recover inexact versions of the minimizing sequences. Therefore, we introduce r_ε^k , δ_ε^k , and u_ε^k to represent the neural networks approximations at each step, where $\varepsilon > 0$ is a tolerance parameter controlling the relative errors of the optimization.

Inexact Approach 1. For the summation scheme, the inexact method is defined as follows:

$$\begin{cases} \text{Given } u^0 \in \mathbb{U}, \text{ let} \\ r_\varepsilon^k \approx r^k := \arg \min_{r \in \mathbb{V}} \frac{1}{2} \|r\|_{\mathbb{V}}^2 - \ell(r) + b(u^k, r); \\ \delta_\varepsilon^k \approx \delta^k := \arg \min_{\delta \in \mathbb{U}} \frac{1}{2} \|\delta\|_{\mathbb{U}}^2 - b(\delta, r_\varepsilon^k); \\ u^{k+1} = u^0 + \rho \delta_\varepsilon^0 + \rho \delta_\varepsilon^1 + \dots + \rho \delta_\varepsilon^k, \end{cases} \quad (26)$$

where we request the optimization process to be sufficiently accurate to bound the relative errors of the residual and the correction, such that

$$\frac{\|r_\varepsilon^k - r^k\|_{\mathbb{V}}}{\|r^k\|_{\mathbb{V}}} \leq \varepsilon \quad \text{and} \quad \frac{\|\delta_\varepsilon^k - \delta^k\|_{\mathbb{U}}}{\|\delta^k\|_{\mathbb{U}}} \leq \varepsilon. \quad (27)$$

The convergence of this inexact method is established in the following theorem, based on the result from [4, Theorem 3.1].

Theorem 1. If $\rho < 2\|B\|^{-2}$ and (27) holds for $\varepsilon > 0$ satisfying $\varepsilon^2 + 2\varepsilon < (1 - \|I - \rho B' B\|)/\rho\|B\|^2$, then the scheme defined in (26) is such that $\{r_\varepsilon^k\} \rightarrow 0_{\mathbb{V}}$, $\{\delta_\varepsilon^k\} \rightarrow 0_{\mathbb{U}}$ and $\{u^k\} \rightarrow u^*$.

Proof. See Appendix A.1. □

Inexact Approach 2. When replacing the summation of Inexact Approach 1 with a minimization of the \mathbb{U} -norm to avoid dynamically expanding the network architecture, the inexact method reads as follows:

$$\left\{ \begin{array}{l} \text{Given } u_\varepsilon^0 \in \mathbb{U}, \text{ let} \\ r_\varepsilon^k \approx r^k := \arg \min_{r \in \mathbb{V}} \frac{1}{2} \|r\|_{\mathbb{V}}^2 - \ell(r) + b(u_\varepsilon^k, r); \\ \delta_\varepsilon^k \approx \delta^k := \arg \min_{\delta \in \mathbb{U}} \frac{1}{2} \|\delta\|_{\mathbb{U}}^2 - b(\delta, r_\varepsilon^k); \\ u_\varepsilon^{k+1} \approx u^{k+1} = \arg \min_{u \in \mathbb{U}} \|u - (u_\varepsilon^k + \rho \delta_\varepsilon^k)\|_{\mathbb{U}}^2. \end{array} \right. \quad (28)$$

The integrand of this final minimization tends to zero if we use a warm-start strategy, initializing the network parameters of u_ε^{k+1} with those from u_ε^k . In addition to the bounds in (27), we must also control the following relative error of this final update:

$$\frac{\|u_\varepsilon^{k+1} - u^{k+1}\|_{\mathbb{U}}}{\|\rho \delta_\varepsilon^k\|_{\mathbb{U}}} \leq \varepsilon. \quad (29)$$

If u_ε^k is poorly trained, the updated function u_ε^{k+1} may not improve the solution, and the error could even increase. The following theorem establishes the convergence of this approach under specific tolerance conditions.

Theorem 2. If $\rho < 2\|B\|^{-2}$ and (27)-(29) hold for $\varepsilon > 0$ satisfying $\varepsilon^3 + 3\varepsilon^2 + 3\varepsilon < (1 - \|I - \rho B' B\|)/\rho\|B\|^2$, then the inexact method (28) satisfies $\{r_\varepsilon^k\} \rightarrow 0_{\mathbb{V}}$, $\{\delta_\varepsilon^k\} \rightarrow 0_{\mathbb{U}}$ and $\{u_\varepsilon^k\} \rightarrow u^*$.

Proof. See Appendix A.2. □

Inexact Approach 3 (Uzawa Deep Double Ritz Method). The inexact version of this two-step scheme corresponds to the method analyzed in [4]. Introducing the neural network approximations r_ε^k and u_ε^k , the method reads:

$$\left\{ \begin{array}{l} r_\varepsilon^k \approx \arg \min_{r \in \mathbb{V}} \frac{1}{2} \|r\|_{\mathbb{V}}^2 - \ell(r) + b(u_\varepsilon^k, r), \\ u_\varepsilon^{k+1} \approx \arg \min_{u \in \mathbb{U}} \frac{1}{2} \|u\|_{\mathbb{U}}^2 - (u_\varepsilon^k, u)_{\mathbb{U}} - \rho b(u, r_\varepsilon^k). \end{array} \right. \quad (30)$$

As established in [4, Theorems 3.1 and 3.2], this iterative scheme converges provided the inexact inner updates satisfy relative error bounds analogous to (27) and (29), ensuring they consistently move in the correct descent direction.

3 Neural Network Architecture and Training

3.1 Architecture

To construct approximations of the trial and test spaces \mathbb{U} and \mathbb{V} , we parameterize the solutions using neural networks. In order to efficiently capture a broad range of frequencies, we employ a modified architecture defined as follows:

A) Layer 1: Fourier Feature Mapping: Let $\mathbf{x} \in \Omega \subset \mathbb{R}^d$ be the input vector. To capture high-frequency features [23], we define the mapping $\gamma_{\boldsymbol{\kappa}} : \Omega \rightarrow \mathbb{R}^n$ using a frequency vector $\boldsymbol{\kappa} = (\kappa_1, \dots, \kappa_n) \in \mathbb{R}^n$ (whose values will be determined in Section 3.2), trainable weights $\mathbf{w}_j \in \mathbb{R}^d$ and biases $b_j \in \mathbb{R}$, for $j = 1, 2, \dots, n$, such that

$$\mathbf{z}_1 = \gamma_{\boldsymbol{\kappa}}(\mathbf{x}) = (\sin(\kappa_1(\mathbf{w}_1^\top \mathbf{x} + b_1)), \dots, \sin(\kappa_n(\mathbf{w}_n^\top \mathbf{x} + b_n))). \quad (31)$$

B) Hidden Layers ($l = 2, \dots, L$): Let σ be a non-linear activation function (e.g., tanh). For each layer l , with trainable weights $\mathbf{W}_l \in \mathbb{R}^{n \times n}$ and biases $\mathbf{b}_l \in \mathbb{R}^n$, we define:

$$\mathbf{z}_l = \sigma(\mathbf{W}_l \mathbf{z}_{l-1} + \mathbf{b}_l). \quad (32)$$

Output Generator Functions. If necessary, to strongly satisfy the homogeneous Dirichlet boundary conditions, we multiply the network output \mathbf{z}_L element-wise by a smooth cut-off function $\xi(\mathbf{x})$ that vanishes on the portion of the boundary where Dirichlet boundary conditions are imposed [5]. This defines the functions $\{\phi_j\}_{j=1}^n$:

$$\phi_j(\mathbf{x}) = (\mathbf{z}_L(\mathbf{x}))_j \cdot \xi(\mathbf{x}). \quad (33)$$

Linear Combination (Output). The final output is the dot product of the vector functions $\boldsymbol{\phi}(\mathbf{x}) = (\phi_1(\mathbf{x}), \dots, \phi_n(\mathbf{x}))^\top$ and a set of output weights $\mathbf{w}_{out} \in \mathbb{R}^n$:

$$v_\theta(\mathbf{x}) = \sum_{j=1}^n w_{out,j} \phi_j(\mathbf{x}) = \mathbf{w}_{out} \boldsymbol{\phi}(\mathbf{x}). \quad (34)$$

The set of trainable parameters is $\theta := \{\mathbf{w}_{out}\} \cup \theta_H$, where $\theta_H := \{\{\mathbf{w}_j, b_j\}_{j=1}^n, \bigcup_{l=2}^L \{\mathbf{W}_l, \mathbf{b}_l\}\}$ denotes the subset of hidden parameters.

3.2 Parameter Initialization via Spectral Analysis

Neural networks suffer from *spectral bias* [10, 17], effectively acting as low-pass filters that favor smooth approximations over high-frequency components. While Fourier Feature Mapping mitigates this issue through tunable frequency parameters $\boldsymbol{\kappa} = (\kappa_1, \dots, \kappa_n)$, standard initialization strategies often fail to target the specific spectral content of the solution. To address this, we employ a data-driven tuning strategy based on the *Power Spectral Density* (PSD) (see, e.g., [9, 14]).

Given a function g evaluated on a discrete computational grid (which in our framework represents either a residual or a Riesz representative), we compute its discrete Fourier transform (DFT) using the Fast Fourier Transform (FFT). To quantify the spectral energy distribution up to a frequency threshold $\eta > 0$, we define the *Normalized Cumulative Power Spectral Density* (NCPSD) as follows:

$$\text{NCPSD}_s(g)(\eta) := \frac{\sum_{|\omega_m| \leq \eta} (1 + |\omega_m|^2)^s |\hat{g}_m|^2}{\sum_{m=1}^M (1 + |\omega_m|^2)^s |\hat{g}_m|^2}, \quad (35)$$

where \hat{g}_m denotes the m -th coefficient of the DFT of g , ω_m is the corresponding discrete angular frequency, M is the number of samples used to discretize g , and $s \in \mathbb{Z}$ is an integer index that dictates frequency weighting.

The choice of the weighting factor $(1 + |\omega_m|^2)^s$ is motivated by Plancherel's theorem. Indeed, the Sobolev norm $\|g\|_{H^s(\mathbb{R}^d)}^2$ of a generic function is equivalent to a frequency-weighted L^2 -norm:

$$\|g\|_{H^s(\mathbb{R}^d)}^2 \cong \int_{\mathbb{R}^d} (1 + |\omega|^2)^s |\hat{g}(\omega)|^2 d\omega. \quad (36)$$

Thus, the integer index s dictates the regularity regime: non-negative values ($s \geq 0$) correspond to standard Sobolev spaces of functions, whereas negative values ($s < 0$) characterize dual spaces of distributions. Although the spectral representation of H^s norms on bounded domains with imposed boundary conditions becomes involved, the discrete estimator defined in (35) acts as a computationally tractable surrogate. In the context of a Poisson-type elliptic problem, we select s explicitly depending on the variational formulation being solved:

- **Strong formulation:** The residual is considered as an element of L^2 ($s = 0$), while the Riesz representative of the correction in the trial space is evaluated in H^2 ($s = 2$).
- **Weak formulation:** The residual is considered as an element of the dual test space H^{-1} ($s = -1$), while the Riesz representative of the correction in the trial space is evaluated in H_0^1 ($s = 1$).
- **Ultra-weak formulation:** The residual is considered as an element of the dual test space H^{-2} ($s = -2$), while the Riesz representative of the correction in the trial space is evaluated in L^2 ($s = 0$).

By analyzing the NCPD, we identify the effective bandwidth $[\omega_{\min}, \omega_{\max}]$ containing a target energy fraction $\alpha \in (0, 1)$ (e.g., $\alpha = 0.05$). To uniquely define this interval and discard negligible energy at both extremes, we truncate the tails of the distribution symmetrically. Specifically, we choose the cut-off frequencies ω_{\min} and ω_{\max} such that:

$$\text{NCPD}_s(g)(\omega_{\min}) = \alpha \quad \text{and} \quad \text{NCPD}_s(g)(\omega_{\max}) = 1 - \alpha. \quad (37)$$

To ensure a multiscale representation, the frequency scalars κ_j are sampled from a log-uniform distribution over this interval, i.e.,

$$\ln(\kappa_j) \sim \mathcal{U}(\ln(\omega_{\min}), \ln(\omega_{\max})). \quad (38)$$

On the other hand, regarding the spatial weights \mathbf{w}_j and biases b_j , we follow the initialization scheme proposed for implicit neural representations [22]. Specifically, \mathbf{w}_j are drawn from a uniform distribution $\mathcal{U}(-1, 1)$ to ensure spectral coverage, while b_j are sampled uniformly in $(-\pi, \pi)$. This combination guarantees that the output generators $\{\phi_j\}_{j=1}^n$ possess the necessary resolving power to approximate the dominant error modes from the onset of training. Finally, for the parameters of the subsequent hidden layers, we employ the Glorot uniform initialization when using the tanh activation function, and the He uniform initialization when employing ReLU³.

3.3 Training: Hybrid LS/Adam with Normalization

The training process aims to find an optimal set of parameters θ that minimize a given loss functional $\mathcal{L}(u_\theta)$. To accelerate convergence, we employ a hybrid optimization strategy that decouples the linear and non-linear parameters (cf. [11, 25]).

Least Squares Step. For a fixed set of hidden trainable parameters θ_H , the functions $\{\phi_j\}_{j=1}^n$ are fixed. We notice that in every case (i.e., strong, weak, ultra-weak) the involved loss function is quadratic with respect to the linear output weights \mathbf{w}_{out} . Hence, each loss can be expressed in algebraic form as:

$$\mathcal{L}(\mathbf{w}_{out}) = \frac{1}{2} \mathbf{w}_{out}^\top \mathbf{H} \mathbf{w}_{out} - \mathbf{f}^\top \mathbf{w}_{out} + q, \quad (39)$$

where $\mathbf{H} \in \mathbb{R}^{n \times n}$ is a Hessian matrix, $\mathbf{f} \in \mathbb{R}^n$ is a load vector, and $q \in \mathbb{R}$ is a scalar. When \mathbf{H} is non-singular, minimizing this quadratic form is equivalent to solving the linear system $\mathbf{H} \mathbf{w}_{out} = \mathbf{f}$.

Output Generators Normalization. The Hessian matrix \mathbf{H} may be singular due to linear dependencies of the output generators. Standard Tikhonov regularization ($\mathbf{H} + \lambda \mathbf{I}$) can be ineffective if the spectrum of \mathbf{H} is arbitrary, as the regularization parameter λ might disproportionately affect relevant eigenvalues or fail to stabilize small ones. To address this, we apply *diagonal scaling* (normalization) to bound the maximum eigenvalue of the system. Let $s_j = \sqrt{\mathbf{H}_{jj}}$ be the scaling factors and $\mathbf{S} = \text{diag}(s_1, \dots, s_n)$.

The normalized system is given by:

$$\tilde{\mathbf{H}} \tilde{\mathbf{w}} = \tilde{\mathbf{f}}, \quad \text{with} \quad \tilde{\mathbf{H}} = \mathbf{S}^{-1} \mathbf{H} \mathbf{S}^{-1}, \quad \tilde{\mathbf{f}} = \mathbf{S}^{-1} \mathbf{f}. \quad (40)$$

This normalization guarantees that the maximum eigenvalue is bounded by the network width ($\lambda_{\max}(\tilde{\mathbf{H}}) \leq \text{Tr}(\tilde{\mathbf{H}}) = n$). Consequently, this spectral bound ensures that the regularization term $\lambda \mathbf{I}$ applied to $\tilde{\mathbf{H}}$ preserves most of the information of the eigenmodes associated with eigenvalues larger than λ . In this way, we solve $(\tilde{\mathbf{H}} + \lambda \mathbf{I}) \tilde{\mathbf{w}} = \tilde{\mathbf{f}}$ and recover the initial weights via $\mathbf{w}_{out} = \mathbf{S}^{-1} \tilde{\mathbf{w}}$.

Adam Step. After updating \mathbf{w}_{out} , we fix the linear layer and perform a gradient descent step (Adam) on the hidden parameters θ_H to minimize $\mathcal{L}(u_{\theta_H})$. Note that, with a slight abuse of notation, we use \mathcal{L} throughout this section to denote the loss evaluated with respect to the specific subset of parameters (or functions) being optimized at each respective step. The complete procedure for a single training iteration, integrating the weight normalization and the alternation between the linear and non-linear updates, is summarized in Algorithm 1.

Algorithm 1 One step of the Hybrid LS/Adam training algorithm

- 1: **Input:** Current hidden trainable parameters θ_H , regularization λ .
 - 2: **1. Least-Squares Step:**
 - 3: Generate $\{\phi_j\}$ and assemble \mathbf{H}, \mathbf{f} such that $\mathcal{L} \approx \frac{1}{2} \mathbf{w}^\top \mathbf{H} \mathbf{w} - \mathbf{f}^\top \mathbf{w}$.
 - 4: Compute scaling $\mathbf{S} = \text{diag}(\sqrt{H_{jj}})$.
 - 5: Solve $(\mathbf{S}^{-1} \mathbf{H} \mathbf{S}^{-1} + \lambda \mathbf{I}) \tilde{\mathbf{w}} = \mathbf{S}^{-1} \mathbf{f}$.
 - 6: Update: $\mathbf{w}_{out} \leftarrow \mathbf{S}^{-1} \tilde{\mathbf{w}}$.
 - 7: **2. Adam Step (Hidden Layers):**
 - 8: Compute $\nabla_{\theta_H} \mathcal{L}$ with updated \mathbf{w}_{out} .
 - 9: Update $\theta_H \leftarrow \text{Adam}(\nabla_{\theta_H} \mathcal{L})$.
-

4 Loss Discretization

All of the above formulations consider losses that require the evaluation of integrals over the computational domain Ω . As shown in [19], employing a deterministic quadrature rule for the Deep Ritz Method (DRM) can lead to catastrophic overfitting. The loss functions used in **Approach 1** (see Section 2.4.1), **Approach 2** (see Section 2.4.2) and **Approach 3** (see Section 2.4.3) are based on the DRM. Furthermore, it is established in [24] that even in the best-case scenario where the optimizer converges to a local minimum, the bias inherent in quadrature rules can yield a poor approximation of the solution. To mitigate these issues, we employ unbiased stochastic quadrature rules. Now, we recall the discussion given in [24].

4.1 Vanilla Monte Carlo

This method approximates the integral by averaging the values of the integrand at a set of N points $\{x_n\}_{n=1}^N$, sampled independently from a uniform distribution on Ω . The approximation is given by:

$$\int_{\Omega} L(x) dx \approx \frac{|\Omega|}{N} \sum_{n=1}^N L(x_n).$$

This quadrature rule provides an unbiased estimator of the integral, i.e.,

$$\mathbb{E} \left[\frac{|\Omega|}{N} \sum_{n=1}^N L(x_n) \right] = \int_{\Omega} L(x) dx.$$

Furthermore, its variance is given by:

$$\text{Var} \left[\frac{|\Omega|}{N} \sum_{n=1}^N L(x_n) \right] = \frac{|\Omega|^2}{N} \text{Var}[L(x)] = \frac{|\Omega|}{N} \int_{\Omega} (L(x))^2 dx - \frac{1}{N} \left(\int_{\Omega} L(x) dx \right)^2. \quad (41)$$

4.2 Stratified Monte Carlo Methods

In this approach, the integration domain Ω —here considered a 1D interval for simplicity—is partitioned into K disjoint subintervals, such that $\Omega = I_1 \sqcup \dots \sqcup I_K$. This methodology can be extended to higher-dimensional meshes. The integral over Ω is decomposed into a sum, where each term is mapped to a common reference interval $I = (-1, 1)$:

$$\int_{\Omega} L(x) dx = \sum_{i=1}^K \int_{I_i} L(x) dx = \sum_{i=1}^K |I_i| \int_I L_i(\hat{x}) d\hat{x}.$$

Here, $L_i(\hat{x})$ denotes the transformed integrand corresponding to the subinterval I_i . The samples within each element must be chosen independently and identically distributed (i.i.d.) and must remain independent across the different subintervals. To approximate the integral over the reference interval, we consider the following unbiased stochastic quadrature rules applied to a generic function $L(\hat{x})$.

Order-3 Unbiased Quadrature Rule (P_3)

A random point x_1 is sampled from the interval $(0, 1)$ according to the probability density function $\mathcal{P}(x) = 3x^2$. The integral is then approximated by the following rule:

$$\int_I L(\hat{x}) d\hat{x} \approx \frac{L(x_1) - 2L(0) + L(-x_1)}{3x_1^2} + 2L(0), \quad \text{where } x_1 \sim \mathcal{P}(x) = 3x^2 \text{ on } (0, 1).$$

Consequently, for a partition of K subintervals, the total number of collocation points is $N_K = 3K$. The quadrature rule is exact for cubic functions (see [21]) and, when L is \mathcal{C}^4 , the variance scales as $\mathcal{O}((N_K)^{-9})$ (cf. [24]).

4.3 Variance Analysis

We analyze the asymptotic behavior of the variance of the stochastic gradient estimators for the three proposed formulations within Approach 1. A key distinction arises between the strong formulation and the variational (weak and ultra-weak) formulations regarding the *passive variance reduction* properties of the gradient of the loss: while in the strong formulation we observe that the variance of the gradient of the loss tends to zero as we converge, this is not the case for the weak and ultra-weak formulations.

Strong Formulation (Approach 1 (S)) In the strong formulation (see Section 2.5.1), the residual of the current iterate u^k is explicitly given by $r^k = f - Bu^k$. The correction δ^k is obtained by minimizing the L^2 -norm of the discrepancy between $B\delta$ and this residual, i.e., $\mathcal{L}(\delta) = \|B\delta - r^k\|_{L^2}^2$. The gradient with respect to the network parameters θ is approximated using Stratified Monte Carlo integration:

$$\nabla_{\theta} \mathcal{L} = \int_{\Omega} (B\delta - r^k) \partial_{\theta} B\delta \, dx \approx \sum_{i=1}^{N_K} 2w_i (B\delta(x_i) - r^k(x_i)) \cdot \partial_{\theta} (B\delta(x_i)).$$

Assuming commutativity of ∂_{θ} and B , as $\delta \in \mathbb{U}$, it holds that $\partial_{\theta} \delta \in \mathbb{U}$, so we may understand $v = B(\partial_{\theta} \delta) \in L^2(\Omega)$ as a test function, so that the gradient of the loss acts like the residual acting on a test function via

$$\nabla_{\theta} \mathcal{L} = \int_{\Omega} (B\delta - r^k) v \, dx \approx \sum_{i=1}^{N_K} 2w_i (B\delta(x_i) - r^k(x_i)) \cdot v(x_i). \quad (42)$$

From this, we estimate the variance assuming that v admits a uniform bound $|v(x)| < C$ and $w_i > 0$ for any $i = 1, \dots, N_K$. We have, via Cauchy-Schwarz

$$\begin{aligned} \mathbb{E} \left(\left| \sum_{i=1}^{N_K} 2w_i (B\delta(x_i) - r^k(x_i)) \cdot v(x_i) \right|^2 \right) &\leq 4 \mathbb{E} \left[\left(\sum_{i=1}^{N_K} w_i |B\delta(x_i) - r^k(x_i)|^2 \right) \left(\sum_{i=1}^{N_K} w_i |v(x_i)|^2 \right) \right] \\ &\leq 4 \sup_{x \in \Omega} |v(x)|^2 \left(\sum_{i=1}^{N_K} w_i \right) \mathbb{E} \left[\sum_{i=1}^{N_K} w_i |B\delta(x_i) - r^k(x_i)|^2 \right] \\ &= 4C^2 |\Omega| \int_{\Omega} |B\delta(x) - r^k(x)|^2 \, dx. \end{aligned}$$

This quantity is an upper bound for the variance, and so we see that the variance decreases as the exact loss decreases, since $B\delta - r^k \rightarrow 0$ in the L_2 norm, thus, yielding a passive reduction of variance.

Weak Formulation (Approach 1 (W)) Consider the loss function $\mathcal{L}(r) = \frac{1}{2}b(r, r) + b(u^k, r) - \ell(r)$. For a standard elliptic operator where $b(u, v) = \int \nabla u \cdot \nabla v$ and $\ell(v) = (f, v)$ the gradient with respect to a trainable parameter θ is given by the integral of:

$$\nabla_{\theta} \mathcal{L} = b(u, v) - \ell(v) = \int_{\Omega} (\nabla u(x) \cdot \nabla v(x) - f(x)v(x)) \, dx, \quad (43)$$

where $v = \partial_{\theta} r$ acts as a test function¹. We denote the Vanilla Monte Carlo rule for this gradient by $\hat{g} = \frac{|\Omega|}{N} \sum_{i=1}^N \nabla_{\theta} L(u_{\theta}(x_i))$. The variance of this estimator is:

$$\text{Var}[\hat{g}] = \frac{|\Omega|^2}{N} \text{Var}[\nabla_{\theta} L(x)] = \frac{|\Omega|^2}{N} (\mathbb{E}[|\nabla_{\theta} L(x)|^2] - |\mathbb{E}[\nabla_{\theta} L(x)]|^2). \quad (44)$$

At the exact solution, the weak form is satisfied; thus, the expected value of the gradient is zero ($\mathbb{E}[g(x)] = 0$). Therefore, the variance reduces to the second moment of the integrand:

$$\text{Var}[\hat{g}] = \frac{|\Omega|}{N} \int_{\Omega} |\nabla u(x) \cdot \nabla v(x) - f(x)v(x)|^2 \, dx. \quad (45)$$

Since the integrand is generally non-zero, the variance remains strictly positive ($\text{Var}[\hat{g}] > 0$) and possibly large, even at the exact solution.

Ultra-weak Formulation (Approach 1 (U)) Similarly, for the ultra-weak formulation, the gradient estimator involves the adjoint operator B' . For the Poisson problem, the gradient with respect to a trainable parameter θ is given by:

$$\nabla_{\theta} \mathcal{L} = (u, B'v)_{L^2} - (f, v)_{L^2} = \int_{\Omega} (-u(x)(\Delta v)(x) - f(x)v(x)) \, dx, \quad (46)$$

where $v = \partial_{\theta} r$. The variance of the Monte Carlo estimator at the exact solution is given by:

$$\text{Var}[\hat{g}] = \frac{|\Omega|}{N} \int_{\Omega} |-u(x)\Delta v(x) - f(x)v(x)|^2 \, dx. \quad (47)$$

Again, the condition $\nabla_{\theta} \mathcal{L} = 0$ (global satisfaction of the ultra-weak form) does not enforce that the integrand vanishes pointwise. Therefore, the stochastic gradient estimator suffers from persistent variance.

5 Numerical Experiments

In this section, we evaluate the performance of the Ritz–Uzawa Neural Networks (RUNNs) framework across different variational settings. Throughout these experiments, we use the arg min operator over the neural network parameters θ to denote the optimal parameters found during the training process. We remark that this constitutes a slight abuse of notation; due to the highly non-linear parameter space and the use of numerical optimizers, the arg min should be understood as the practical approximation obtained after training, rather than a strict global minimum.

5.1 Weak Formulation: The Poisson Problem

We consider the domain $\Omega = (-1, 1) \subset \mathbb{R}$ and the Poisson problem with homogeneous Dirichlet boundary conditions:

$$\begin{cases} -u'' = f & \text{in } \Omega, \\ u(-1) = u(1) = 0, \end{cases} \quad (48)$$

where the source term f is chosen such that the exact manufactured solution is known. We employ the Sobolev spaces $\mathbb{U} = \mathbb{V} = H_0^1(\Omega)$, with the weak bilinear form $b(u, v) = (u', v')_{L_2(\Omega)}$ and the linear functional $\ell(v) = (f, v)_{L_2(\Omega)}$.

¹It is crucial to note that the convergence of the residual $r \rightarrow 0$ does not imply that its sensitivity with respect to the parameters vanishes (i.e., $v = \partial_{\theta} r \not\rightarrow 0$). For instance, if $r(x; \theta) = \theta \phi(x)$ with $-\Delta \phi = f$, then at the optimum $\theta = 0$, the residual vanishes but the test function $v = \phi$ does not, generating variance even at the exact solution.

Explicit Loss Formulation and Iterative Scheme. Following Approach 1 (W), the solution is constructed iteratively via the Uzawa scheme by minimizing a sequence of concrete energy functionals. First, the initial ansatz u^0 is obtained by the standard Deep Ritz Method:

$$u^0 = \arg \min_{u_\theta} \mathcal{L}(u_\theta) := \arg \min_{u_\theta} \int_{\Omega} \left[\frac{1}{2} (u'_\theta(x))^2 - f(x)u_\theta(x) \right] dx. \quad (49)$$

Subsequently, for each iteration $k \geq 0$, the correction r^k is computed by minimizing the residual energy, and the overall solution is updated as $u^{k+1} = u^k + r^k$ (denoted algorithmically as $u^{k+1} \leftarrow u^k + r^k$ in the subsequent figures). The functional for this correction step is given by:

$$r^k = \arg \min_{r_\theta} \mathcal{L}_k(r_\theta) := \arg \min_{r_\theta} \int_{\Omega} \left[\frac{1}{2} (r'_\theta(x))^2 + (u^k)'(x)r'_\theta(x) - f(x)r_\theta(x) \right] dx. \quad (50)$$

Minimizing $\mathcal{L}_k(r_\theta)$ is equivalent to finding $\arg \min_{r_\theta} \frac{1}{2} \|r_\theta - e^k\|_{H_0^1(\Omega)}^2$, where $e^k = u^* - u^k$ is the exact error.

Neural Network Ansatz. To approximate the solution, we employ a neural network ansatz $u_\theta(x)$ as defined in Section 3, explicitly selecting the smooth cut-off function $\xi(x) = (1 - x^2)$ to strongly satisfy the boundary conditions by design. The specific network configuration varies depending on the complexity of the solution:

- **Shallow Configuration ($L = 1$):** For the smooth solutions analyzed in Sections 5.1.1 and 5.1.2, we use a network with 30 neurons serving as Fourier feature generators, and no additional hidden processing layers. This acts strictly as a tunable Fourier basis.
- **Deep Configuration ($L = 2$):** For the high-frequency problem addressed in Section 5.1.3, we employ a network with 30 neurons acting as Fourier feature generators, followed by one hidden layer equipped with a tanh activation function.

Spectral Initialization Strategy. To ensure the neural network frequencies are correctly tuned at each phase of the algorithm, we apply a consistent spectral initialization strategy across all experiments in this section:

- **Initialization of u^0 :** We analyze the source term f . Since f naturally resides in the dual space H^{-1} for a second-order elliptic problem, we compute its Normalized Cumulative Power Spectral Density (NCPSPD) defined in (35) using a regularity index $s = -1$.
- **Initialization of r^0 :** After training u^0 , we lack a prior weak residual to analyze for the first correction. However, since $-(r^0)'' = (u^0)'' + f$ holds in the weak sense, we evaluate the strong residual $(u^0)'' + f$ and compute its NCPSPD using $s = -1$.
- **Initialization of r^k ($k \geq 1$):** For subsequent Uzawa iterative steps, we analyze the previously trained weak residual representative r^{k-1} . Because r^{k-1} belongs to the test space $\mathbb{V} = H_0^1$ and approximates the error in the energy norm, we compute its NCPSPD using $s = 1$.

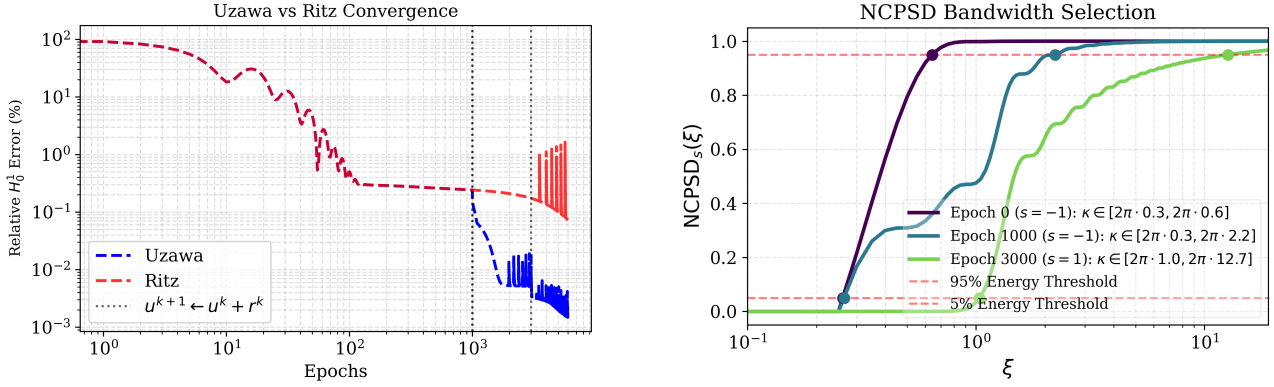
We employ a high-density P_3 quadrature rule (as detailed in Section 4) across all experiments to accurately evaluate these distributions and compute the loss functions. The specific training schedules (epochs, collocation points, and learning rates) are detailed in the respective tables for each experiment.

5.1.1 Baseline with Adam Optimization

Our initial experiment targets the smooth manufactured solution $u^*(x) = \sin(\pi x)$. We employ the standard Adam optimizer alongside the Shallow Configuration to train both the initial guess u^0 and the subsequent iterative corrections r^k , adhering to the training schedule detailed in Table 1. The evolution of the relative error and the corresponding NCPSPD analysis to select $[\omega_{\min}, \omega_{\max}]$ are captured in Figure 1. Providing deeper insight into the correction mechanism, Figure 2 demonstrates that the method successfully approximates the exact error function e^0 and its derivative. However, while the approach ultimately yields a highly accurate final error function (Figure 3), this pure Adam optimization strategy exhibits noticeably slower convergence when compared to the hybrid methods explored in subsequent sections.

Iteration	Phase	Points (N_K)	Epochs	Learning Rate
$k = 0$ (Initial)	u^0	9000	1000	$9 \cdot 10^{-3}$
$k = 1$	r^0	9000	2000	10^{-4}
$k = 2$	r^1	9000	3000	10^{-5}

Table 1: Training hyperparameters for the pure Adam experiment.



(a) Relative error evolution (6,000 epochs).

(b) NCPD bandwidth selection.

Figure 1: Experimental results with Adam: (a) Relative error and (b) The NCPD analysis.

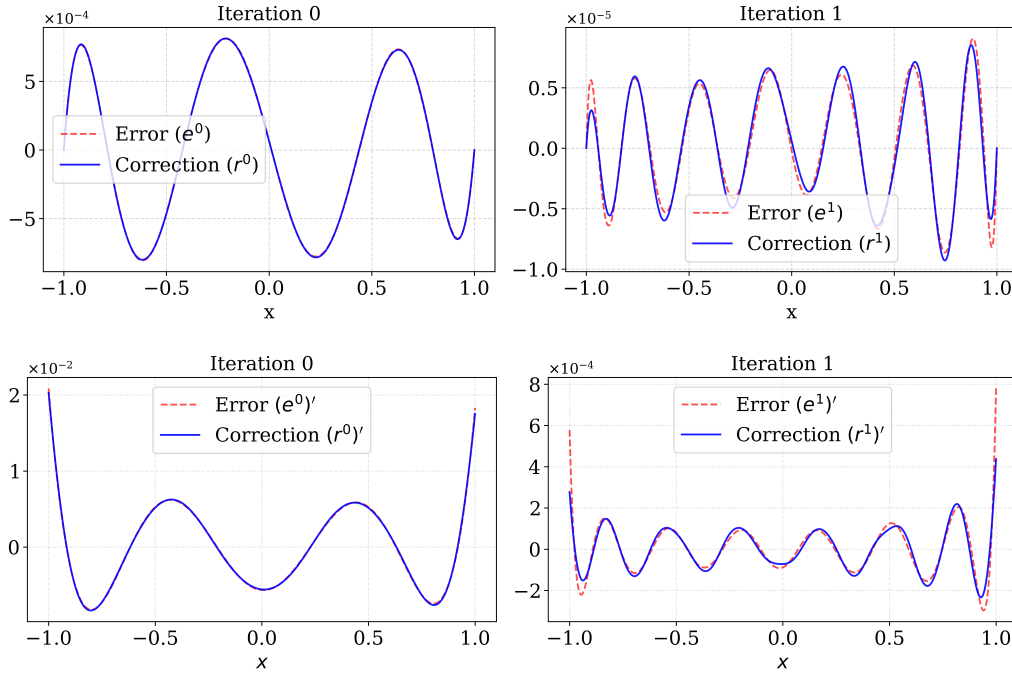


Figure 2: Analysis of the correction step ($k = 0$) after 6,000 epochs. Top: Comparison between the true error e^0 and the learned correction r^0 . Bottom: Comparison of their derivatives.

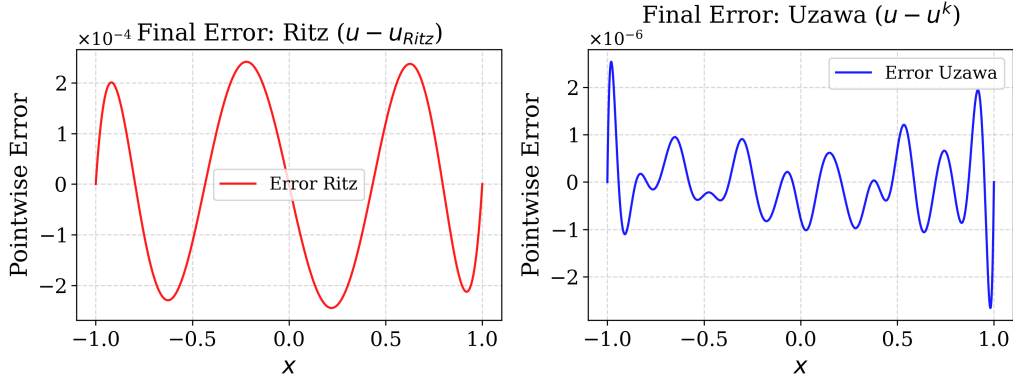


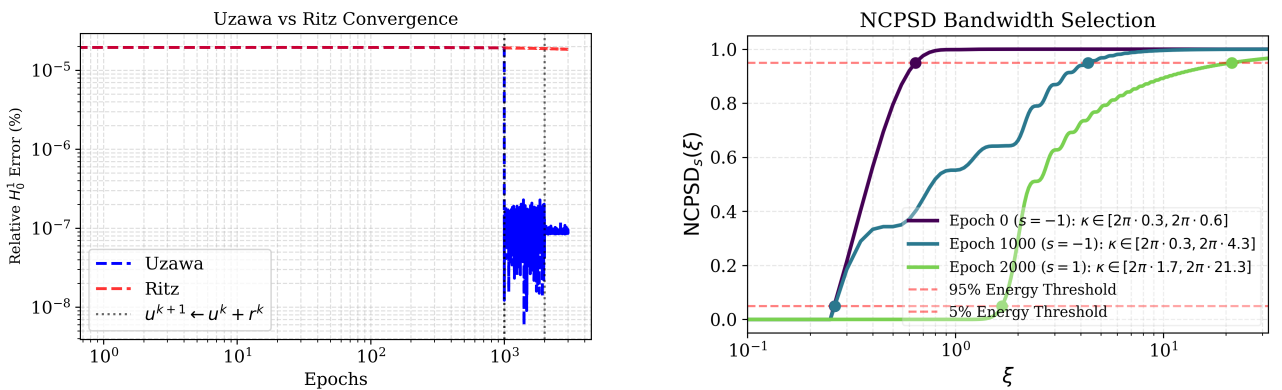
Figure 3: Final error function.

5.1.2 Acceleration with Hybrid LS/Adam

To accelerate convergence, we repeat the baseline experiment using the Hybrid LS/Adam optimizer, maintaining the Shallow Configuration for both the initial guess and its iterative corrections. By alternating between least-squares projections for the linear weights and Adam updates for the hidden parameters (detailed in Table 2), the method achieves a rapid reduction in the relative H_0^1 norm (Figure 4a). Concurrently, the Uzawa-based spectral matching successfully isolates higher-frequency modes (Figure 4b). The efficacy of this correction mechanism is validated in Figure 5, which demonstrates a strong agreement between the residual r^k and the exact error e^k alongside their derivatives, ultimately resulting in the highly accurate final error function shown in Figure 6.

Iteration	Phase	Points (N_K)	Epochs	Learning Rate
$k = 0$ (Initial)	u^0	9000	1000	10^{-2}
$k = 1$	r^0	9000	1000	10^{-3}
$k = 2$	r^1	9000	1000	10^{-3}

Table 2: Training hyperparameters (Hybrid LS/Adam). In this setup, both the Gradient step (Adam) and the Least Squares step utilize the same density of collocation points.



(a) Relative error evolution (3,000 total epochs).

(b) NCPD bandwidth selection.

Figure 4: Experimental results with LS/Adam: (a) Relative error and (b) The NCPD analysis.

As shown in Figure 4, the LS/Adam strategy drastically reduces the training epochs, achieving superior accuracy in 3,000 total epochs compared to the Adam optimization.

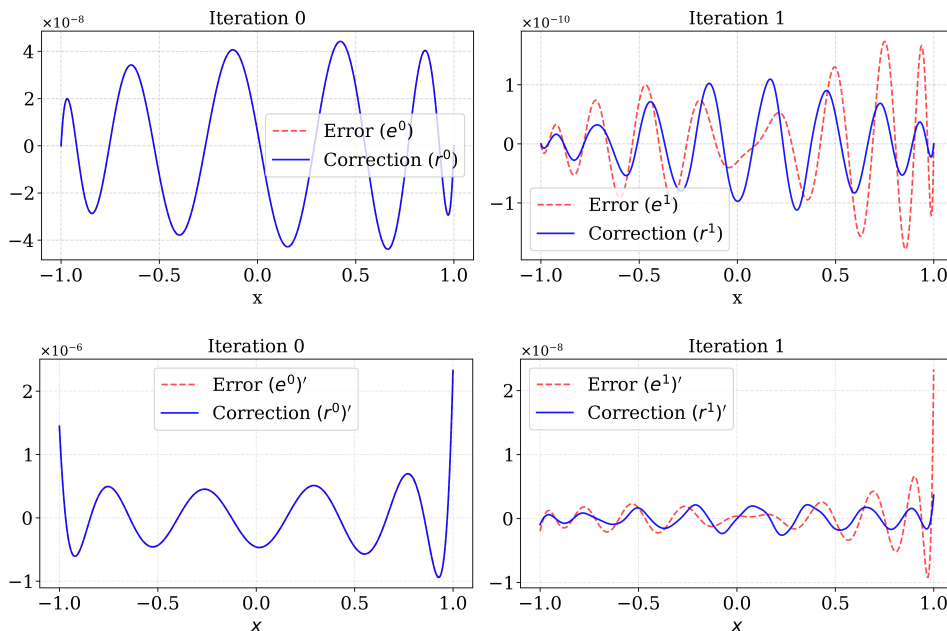


Figure 5: Analysis of the correction step ($k = 0$) after 3,000 epochs. Top: Comparison between the true error e^0 and the learned correction r^0 . Bottom: Comparison of their derivatives.

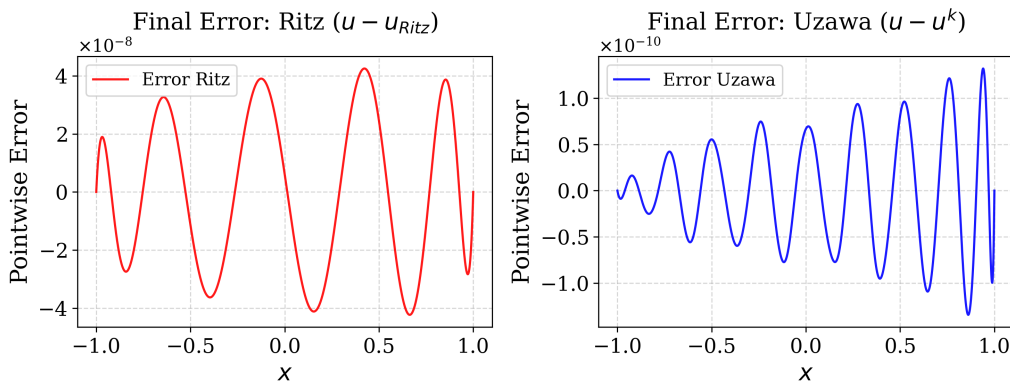


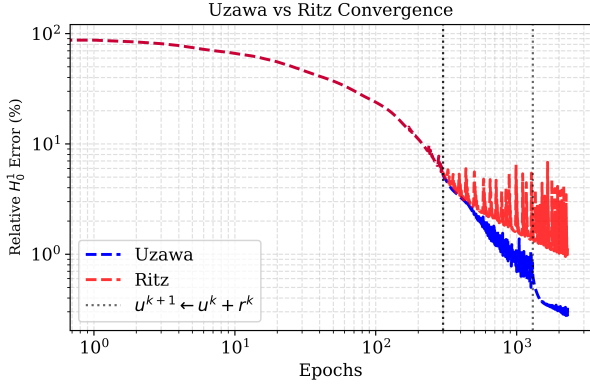
Figure 6: Final error function.

5.1.3 High-Frequency Resolution via Spectral Matching

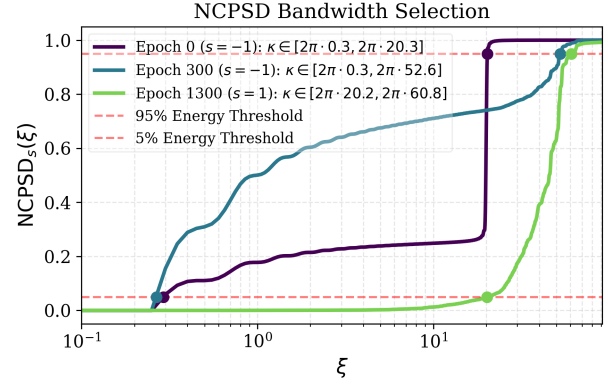
In this experiment, we evaluate the method using the high-frequency manufactured solution $u^*(x) = \sin(40\pi x)$ to address spectral bias. The model is trained using the hybrid LS/Adam optimizer with the hyperparameters detailed in Table 3. Figure 7 shows how we select the bandwidth $[\omega_{\min}, \omega_{\max}]$. Furthermore, Figure 8 shows that the hybrid architecture captures the high-frequency oscillations of the error, resulting in the final pointwise error presented in Figure 9.

Iteration	Phase	Points (N_K)	Epochs	Learning Rate
$k = 0$ (Initial)	u^0	9000	300	10^{-3}
$k = 1$	r^0	9000	1000	10^{-3}
$k = 2$	r^1	9000	1000	10^{-3}

Table 3: Training hyperparameters.



(a) Relative error evolution.



(b) NCPSPD bandwidth selection.

Figure 7: Experimental results for the high-frequency case: (a) Relative error. (b) The NCPSPD bandwidth selection.

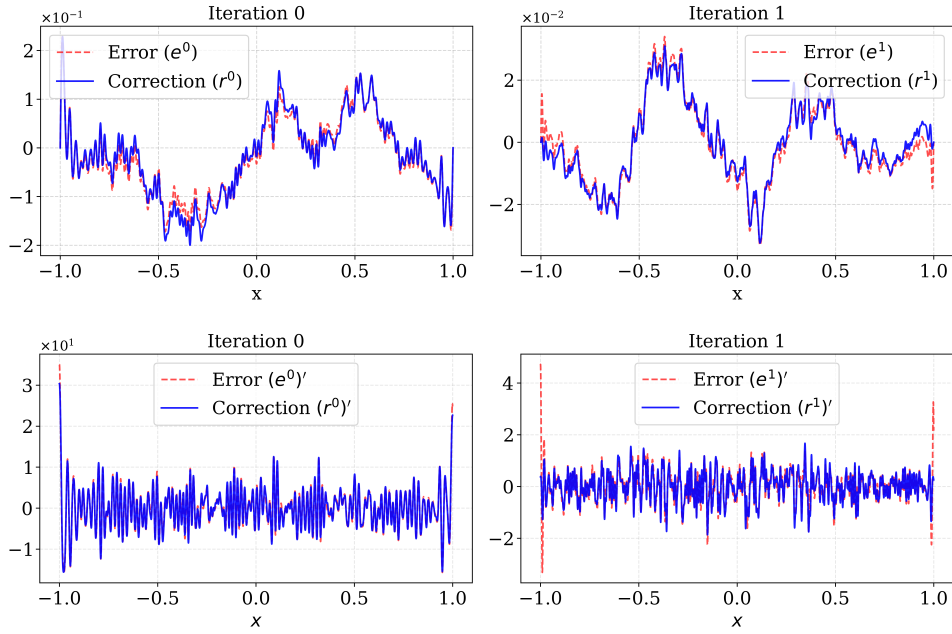


Figure 8: Detailed correction analysis for $u^*(x) = \sin(40\pi x)$. The hybrid architecture captures the high-frequency oscillations of the error e^0 .

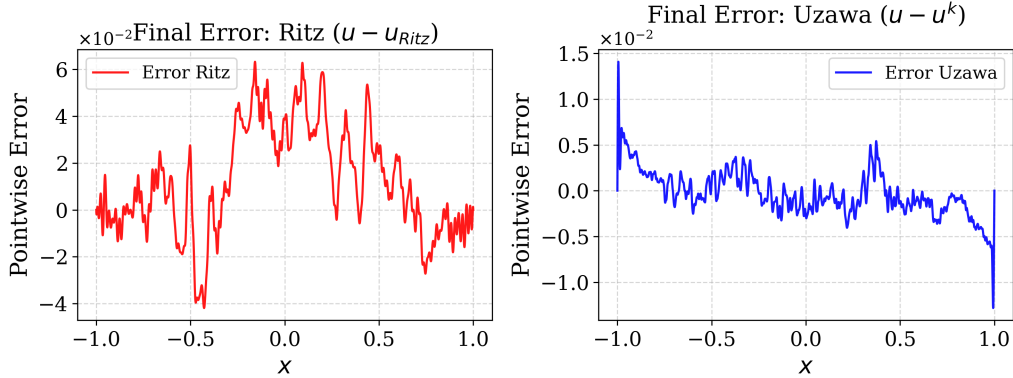


Figure 9: Final pointwise error for the high-frequency experiment.

5.2 Ultra-weak formulation with an H^{-2} source term

We consider the domain $\Omega = (-1, 1) \subset \mathbb{R}$ and the boundary value problem governed by a distributional source term:

$$\begin{cases} -u'' = \delta' & \text{in } \Omega, \\ u(-1) = u(1) = 0. \end{cases} \quad (51)$$

Here, δ' denotes the distributional derivative of the Dirac delta. The exact solution is $u^*(x) = \frac{1}{2}(x+1) - H(x)$, where $H(x)$ is the Heaviside step function. We follow Approach 1 (U) with $\mathbb{U} = L_2(\Omega)$ and $\mathbb{V} = \dot{H}_0^1(\Omega) \cap H^2(\Omega)$.

Explicit Loss Formulation. Following Approach 1 (U), we minimize the energy of the test functions to iteratively recover the primal solution, observing that the test-to-trial operator in this setting acts as $B'v = -v''$. First, the initial test function approximation v is obtained by minimizing the Adjoint Ritz functional:

$$v = \arg \min_{v_\theta} \int_{\Omega} \frac{1}{2} (v_\theta''(x))^2 dx + v_\theta'(0). \quad (52)$$

The initial primal ansatz is then recovered via $u^0 = B'v = -(v)''$. Subsequently, for each iteration $k \geq 0$, the correction test function r^k is computed by minimizing the Uzawa loss, which explicitly incorporates the previous primal approximation u^k :

$$r^k = \arg \min_{r_\theta} \int_{\Omega} \left[\frac{1}{2} (r_\theta''(x))^2 + u^k(x) r_\theta''(x) \right] dx + r_\theta'(0). \quad (53)$$

Note that the isolated derivative terms ($v_\theta'(0)$ and $r_\theta'(0)$) arise from the duality pairing $\langle \delta', \phi \rangle := -\phi'(0)$, which appears with a negative sign ($-\ell(\phi)$) in the respective energy functionals. Finally, following the Uzawa scheme, the primal solution is updated as $u^{k+1} = u^k + B'r^k = u^k - (r^k)''$. In the algorithmic context of the figures, this step is denoted as $u^{k+1} \leftarrow u^k + \delta^k$, where $\delta^k = -(r^k)''$ represents the effective correction in the trial space.

Neural Network Ansatz. To ensure that the neural network output is H^2 -continuous (as strictly required by the test space), the initial approximation $u^0 = -(v)''$ is calculated using a shallow neural network v_θ equipped with cubic ReLU activations (ReLU³). For subsequent Uzawa iterations, the corrections r^k are calculated using a neural network composed of two layers: the first layer is a Fourier feature mapping and the second layer is a ReLU³ network with 30 neurons.

Spectral Initialization Strategy. For the distributional source $f = \delta' \in H^{-2}$, the H^{-2} -weighted energy spectrum decays slowly, reflecting a heavy high-frequency tail. This severe lack of regularity makes it difficult for standard networks to capture the jump discontinuity. We apply the following spectral initialization strategy:

- **Initialization of r^0 :** To tune the frequencies for the first correction, we evaluate the highly singular strong residual $-(u^0)'' - f$ and compute its NCPSPD, also utilizing the regularity index $s = -2$.

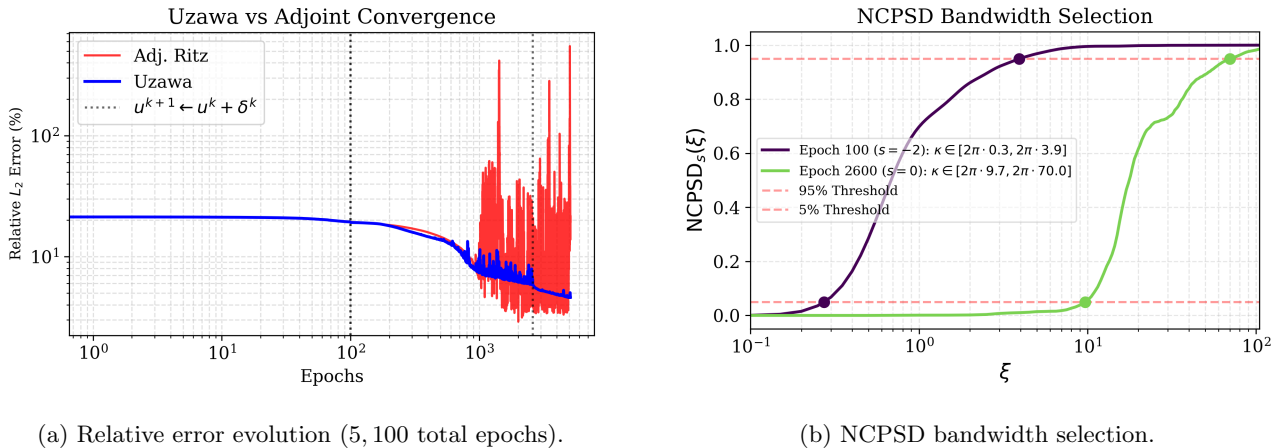
- **Initialization of r^k ($k \geq 1$):** For subsequent Uzawa iterative steps, we rely on the previously trained adjoint test functions. Specifically, we compute the NCPSP directly on the previous primal correction proxy $-(r^{k-1})''$. To capture its spectral energy distribution effectively without over-weighting the singularities, we evaluate the NCPSP in the L^2 norm by setting $s = 0$.

5.2.1 Singularity Resolution via Adjoint Iterations

The model is trained using the hybrid LS/Adam optimizer with the hyperparameters detailed in Table 4. Figure 10a illustrates the relative error in the L^2 norm, and the bandwidth selection $[\omega_{\min}, \omega_{\max}]$ in the NCPSP analysis is shown in Figure 10b. The correction mechanism is analyzed in Figure 11, showing that the network identifies the error distribution e^k through the learned correction $-(r^k)''$, capturing the jump discontinuity at $x = 0$. The final pointwise error is presented in Figure 12.

Iteration	Phase	Points (N_K)	Epochs	Learning Rate
$k = 0$ (Init)	u^0	3000	100	$8 \cdot 10^{-5}$
$k = 1$	r^0	4500	2500	$8 \cdot 10^{-5}$
$k = 2$	r^1	6000	2500	$8 \cdot 10^{-5}$

Table 4: Training hyperparameters for the ultra-weak experiment.



(a) Relative error evolution (5, 100 total epochs).

(b) NCPSP bandwidth selection.

Figure 10: Experimental results for the ultra-weak formulation: (a) Relative error evolution and (b) Evolution of the NCPSP.

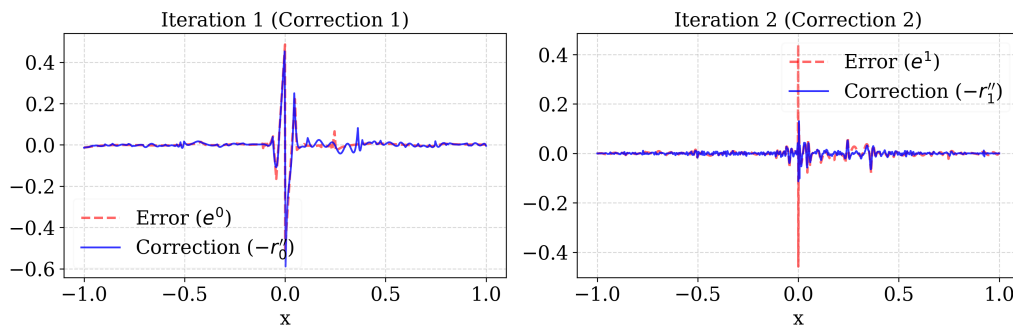


Figure 11: Correction step. The plot compares the true error e^k (red dashed line) with the learned correction $-(r^k)''$ (blue solid line).

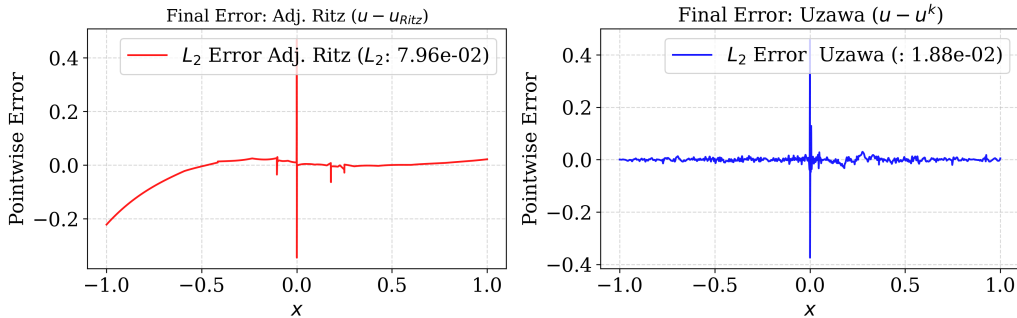


Figure 12: Final pointwise error.

6 Conclusions and Future Work

In this paper, we introduced the Ritz–Uzawa Neural Networks (RUNNs) framework, an iterative methodology to solve Partial Differential Equations (PDEs) across strong, weak, and ultra-weak variational formulations. By reformulating the variational problem as a sequence of Ritz-type minimizations within an inexact Uzawa loop, our approach addresses the instability common in standard neural network solvers. Theoretical analysis and numerical experiments confirm that this iterative scheme, combined with a high-density, unbiased stratified stochastic quadrature rule (P_3), converges to the solution. Furthermore, we show that the strong formulation provides a passive variance reduction mechanism, while the variance remains persistent in weak and ultra-weak regimes.

To address the spectral bias of standard neural networks, we implemented a data-driven frequency tuning strategy. By dynamically initializing a Sinusoidal Fourier Feature Mapping based on the Normalized Cumulative Power Spectral Density (NCPSD) of the residuals, the network adapts its spectral bandwidth to capture high-frequency components and severe singularities. Combined with a hybrid Least Squares/Adam (LS/Adam) optimization scheme, the RUNNs framework significantly accelerates convergence compared to first order gradient descent methods like Adam.

Numerical results demonstrate the robustness of RUNNs across different regularity regimes. The framework accurately resolved highly oscillatory solutions via spectral matching and successfully recovered a discontinuous L^2 solution from a distributional H^{-2} source term using the ultra-weak formulation, a scenario where standard energy-based methods fail. These findings establish the Ritz–Uzawa iterative scheme as a stable and adaptable mesh-free solver. Future work will extend this framework to non-linear PDEs, higher-dimensional geometries, and time-dependent equations, where dynamic spectral tuning and variance-reduction iterations could offer substantial computational advantages.

Acknowledgments Pablo Herrera has received financial support from the Dirección de Investigación (DI), under the Vicerrectoría de Investigación, Creación e Innovación (VINCI) of the Pontificia Universidad Católica de Valparaíso (PUCV), through the 2024 Postdoctoral Fellowship. Jamie M. Taylor has received funding from the following Research Projects: PID2023-146678OB-I00 funded by MICIU/AEI /10.13039/501100011033. Carlos Uriarte is supported by the Postdoctoral Program for the Improvement of Doctoral Research Personnel of the Basque Government (Ref. No. POS-2024-1-0004) and by the Research Projects PID2023-146678OB-I00 and PID2023-146668OA-I00, both funded by MICIU/AEI /10.13039/501100011033. Ignacio Muga is supported by the Chilean National Agency for Research and Development through the Fondecyt Project #1230091. David Pardo has received funding from the following Research Projects/Grants: European Union’s Horizon Europe research and innovation programme under the Marie Skłodowska-Curie Action MSCA-DN-101119556 (IN-DEEP). PID2023-146678OB-I00 funded by MICIU/AEI /10.13039/501100011033 and by FEDER, EU; BCAM Severo Ochoa accreditation of excellence CEX2021-001142-S funded by MICIU / AEI / 10.13039/501100011033; Basque Government through the BERC 2022-2025 program; BEREZ-IA (KK-2023/00012) and RUL-ET(KK-2024/00086), funded by the Basque Government through ELKARTEK; Consolidated Research Group MATH-MODE (IT1866-26) of the UPV/EHU given by the Department of Education of the Basque Government; BCAM- IKUR-UPV/EHU, funded by the Basque Government IKUR Strategy and by the European Union NextGenerationEU/PRTR. The research of Kristoffer van der Zee was supported by the Engineering and Physical Sciences

References

- [1] Z. ALDIRANY, R. COTTEREAU, M. LAFOREST, AND S. PRUDHOMME, *Multi-level neural networks for accurate solutions of boundary-value problems*, Computer Methods in Applied Mechanics and Engineering, 419 (2024), p. 116666.
- [2] H. ALSOBHI, E. BENNY-CHACKO, I. BREVIS, AND K. G. VAN DER ZEE, *Neural network dual norms for minimal residual finite element methods*, arXiv preprint arXiv:2509.16961, (2025).
- [3] C. BACUTA, *A unified approach for Uzawa algorithms*, SIAM Journal on Numerical Analysis, 44 (2006), pp. 2633–2649.
- [4] E. BENNY-CHACKO, I. BREVIS, L. ESPATH, AND K. G. VAN DER ZEE, *Inexact Uzawa-double Deep Ritz Method for weak adversarial neural networks*, arXiv preprint arXiv:2512.05673, (2025).
- [5] S. BERRONE AND M. PINTORE, *Enforcing Dirichlet boundary conditions in physics-informed neural networks via a cut-off function*, Heliyon, 9 (2023), p. e18739.
- [6] J. H. BRAMBLE, J. E. PASCIAK, AND A. T. VASSILEV, *Analysis of the inexact Uzawa algorithm for saddle point problems*, SIAM Journal on Numerical Analysis, 34 (1997), pp. 1072–1092.
- [7] I. BREVIS, I. MUGA, AND K. G. VAN DER ZEE, *A machine-learning minimal-residual (ML-MRes) framework for goal-oriented finite element discretizations*, Computers & Mathematics with Applications, 95 (2021), pp. 186–199.
- [8] H. BREZIS, *Functional Analysis, Sobolev Spaces and Partial Differential Equations*, Universitext, Springer Science & Business Media, New York, NY, 2010.
- [9] S. L. BRUNTON AND J. N. KUTZ, *Data-Driven Science and Engineering: Machine Learning, Dynamical Systems, and Control*, Cambridge University Press, Cambridge, UK, 2022.
- [10] Y. CAO, Z. FANG, Y. WU, D.-X. ZHOU, AND Q. GU, *Towards understanding the spectral bias of deep learning*, in Proceedings of the 30th International Joint Conference on Artificial Intelligence (IJCAI), 2021, pp. 2205–2211.
- [11] E. C. CYR, M. A. GULIAN, R. G. PATEL, M. PEREGO, AND N. A. TRASK, *Robust training and initialization of deep neural networks: An adaptive basis viewpoint*, ArXiv, abs/1912.04862 (2019).
- [12] W. E AND B. YU, *The Deep Ritz Method: Deep learning-based numerical algorithm for solving variational problems*, Communications in Mathematics and Statistics, 6 (2018), pp. 1–12.
- [13] A. ERN AND J.-L. GUERMOND, *Finite Elements II: Galerkin Approximation, Elliptic and Mixed PDEs*, vol. 73 of Texts in Applied Mathematics, Springer International Publishing, Cham, 2021.
- [14] W. KIM, J.-S. HWANG, D.-K. KWON, AND A. KAREEM, *Cumulative power spectral density-based damping estimation*, Earthquake Engineering & Structural Dynamics, 53 (2024), pp. 1787–1802.
- [15] D. P. KINGMA AND J. BA, *Adam: A method for stochastic optimization*, arXiv preprint arXiv:1412.6980, (2017).
- [16] C. G. MAKRIDAKIS, A. PIM, AND T. PRYER, *Deep Uzawa for PDE constrained optimisation*, arXiv preprint arXiv:2410.17359, (2024).
- [17] N. RAHAMAN, A. BARATIN, D. ARPIT, F. DRAXLER, M. LIN, F. HAMPRECHT, Y. BENGIO, AND A. COURVILLE, *On the spectral bias of neural networks*, in Proceedings of the 36th International Conference on Machine Learning (ICML), vol. 97 of PMLR, 2019, pp. 5301–5310.
- [18] M. RAISSI, P. PERDIKARIS, AND G. E. KARNIADAKIS, *Physics-informed neural networks: A deep learning framework for solving forward and inverse problems involving nonlinear partial differential equations*, Journal of Computational Physics, 378 (2019), pp. 686–707.

- [19] J. A. RIVERA, J. M. TAYLOR, ÁNGEL J. OMELLA, AND D. PARDO, *On quadrature rules for solving partial differential equations using neural networks*, Computer Methods in Applied Mechanics and Engineering, 393 (2022), p. 114710.
- [20] S. ROJAS ET AL., *Robust variational physics-informed neural networks*, Computer Methods in Applied Mechanics and Engineering, 425 (2024), p. 116904.
- [21] A. F. SIEGEL AND F. O'BRIEN, *Unbiased Monte Carlo integration methods with exactness for low order polynomials*, SIAM Journal on Scientific and Statistical Computing, 6 (1985), pp. 169–181.
- [22] V. SITZMANN, J. N. P. MARTEL, A. W. BERGMAN, D. B. LINDELL, AND G. WETZSTEIN, *Implicit neural representations with periodic activation functions*, Advances in Neural Information Processing Systems, 33 (2020), pp. 7462–7473.
- [23] M. TANCİK, P. P. SRINIVASAN, B. MILDENHALL, S. FRIDOVICH-KEIL, N. RAGHAVAN, U. SINGHAL, R. RAMAMOORTHY, J. T. BARRON, AND R. NG, *Fourier features let networks learn high frequency functions in low dimensional domains*, in Advances in Neural Information Processing Systems (NeurIPS), vol. 33, 2020, pp. 7537–7547.
- [24] J. M. TAYLOR AND D. PARDO, *Stochastic quadrature rules for solving PDEs using neural networks*, arXiv preprint arXiv:2504.11976v2, (2025).
- [25] C. URIARTE, M. BASTIDAS, D. PARDO, J. M. TAYLOR, AND S. ROJAS, *Optimizing variational physics-informed neural networks using least squares*, Computers & Mathematics with Applications, 185 (2025), pp. 76–93.
- [26] C. URIARTE, D. PARDO, I. MUGA, AND J. MUÑOZ-MATUTE, *A deep double Ritz method (D2RM) for solving partial differential equations using neural networks*, Computer Methods in Applied Mechanics and Engineering, 405 (2023), p. 115892.
- [27] H. UZAWA, *Iterative methods for concave programming*, in Studies in linear and nonlinear programming, Stanford University Press, 1958, pp. 154–165.
- [28] S. WANG, Y. DENG, AND P. PERDIKARIS, *Surpassing the spectral bias of physics-informed neural networks with variational residuals*, arXiv preprint arXiv:2307.08934, (2023).

A Proof of main theorems

A.1 Proof of Theorem 1

Since $\rho < 2\|B\|^{-2}$, by Proposition 2 we have that $\|I - \rho B'B\| < 1$. Thus, $1 - \|I - \rho B'B\|$ is positive.

Let us define $e^k = u^k - u^*$. First, observe that $r^k = B(u^* - u^k) = -Be^k$. Hence, using (27) and triangular inequality, we have:

$$\|r_\varepsilon^k\|_{\mathbb{V}} \leq \|r_\varepsilon^k - r^k\|_{\mathbb{V}} + \|r^k\|_{\mathbb{V}} \leq (\varepsilon + 1)\|r^k\|_{\mathbb{V}} \leq (\varepsilon + 1)\|B\|\|e^k\|_{\mathbb{U}}. \quad (54)$$

Moreover,

$$\|\delta_\varepsilon^k\|_{\mathbb{U}} \leq \|\delta_\varepsilon^k - \delta^k\|_{\mathbb{U}} + \|\delta^k\|_{\mathbb{U}} \leq (\varepsilon + 1)\|\delta^k\|_{\mathbb{U}} = (\varepsilon + 1)\|B'r_\varepsilon^k\|_{\mathbb{U}} \leq (1 + \varepsilon)^2\|B\|^2\|e^k\|_{\mathbb{U}}. \quad (55)$$

Thus, it is enough to prove that $\{e^k\}$ is a contraction. Notice that

$$\begin{aligned} e^{k+1} &= u^{k+1} - u^* \\ &= u^k + \rho\delta_\varepsilon^k - u^* \\ &= e^k + \rho(\delta_\varepsilon^k - \delta^k) + \rho\delta^k \\ &= e^k + \rho(\delta_\varepsilon^k - \delta^k) + \rho B'r_\varepsilon^k \\ &= e^k + \rho(\delta_\varepsilon^k - \delta^k) + \rho B'(r_\varepsilon^k - r^k) + \rho B'r^k \\ &= (I - \rho B'B)e^k + \rho(\delta_\varepsilon^k - \delta^k) + \rho B'(r_\varepsilon^k - r^k). \end{aligned}$$

Therefore,

$$\begin{aligned} \|e^{k+1}\|_{\mathbb{U}} &\leq \|I - \rho B'B\|\|e^k\|_{\mathbb{U}} + \rho\varepsilon(\|\delta^k\|_{\mathbb{U}} + \|B\|\|r^k\|_{\mathbb{V}}) \\ &\leq (\|I - \rho B'B\| + \rho(\varepsilon^2 + 2\varepsilon)\|B\|^2)\|e^k\|_{\mathbb{U}}. \end{aligned}$$

By the hypothesis of the Theorem, the constant $\|I - \rho B'B\| + \rho(\varepsilon^2 + 2\varepsilon)\|B\|^2$ is less than 1, which proves that $\{e^k\}$ is a contraction.

A.2 Proof of Theorem 2

Let us define $e_\varepsilon^k = u_\varepsilon^k - u^*$ and observe that $r^k = B(u^* - u_\varepsilon^k) = -Be_\varepsilon^k$. Analogously to (54) and (55), we have:

$$\|r_\varepsilon^k\|_{\mathbb{V}} \leq (\varepsilon + 1)\|B\|\|e_\varepsilon^k\|_{\mathbb{U}} \quad \text{and} \quad \|\delta_\varepsilon^k\|_{\mathbb{U}} \leq (1 + \varepsilon)^2\|B\|^2\|e_\varepsilon^k\|_{\mathbb{U}}.$$

Thus, it remains to prove that $\{e_\varepsilon^k\}$ is a contraction. Notice that:

$$\begin{aligned} e_\varepsilon^{k+1} &= u_\varepsilon^{k+1} - u^* \\ &= u_\varepsilon^{k+1} - u^{k+1} + u_\varepsilon^k + \rho\delta_\varepsilon^k - u^* \\ &= u_\varepsilon^{k+1} - u^{k+1} + e_\varepsilon^k + \rho(\delta_\varepsilon^k - \delta^k) + \rho\delta^k \\ &= u_\varepsilon^{k+1} - u^{k+1} + e_\varepsilon^k + \rho(\delta_\varepsilon^k - \delta^k) + \rho B'r_\varepsilon^k \\ &= u_\varepsilon^{k+1} - u^{k+1} + e_\varepsilon^k + \rho(\delta_\varepsilon^k - \delta^k) + \rho B'(r_\varepsilon^k - r^k) + \rho B'r^k \\ &= u_\varepsilon^{k+1} - u^{k+1} + (I - \rho B'B)e_\varepsilon^k + \rho(\delta_\varepsilon^k - \delta^k) + \rho B'(r_\varepsilon^k - r^k). \end{aligned}$$

Therefore,

$$\begin{aligned} \|e_\varepsilon^{k+1}\|_{\mathbb{U}} &\leq \rho\varepsilon\|\delta_\varepsilon^k\|_{\mathbb{U}} + \|I - \rho B'B\|\|e_\varepsilon^k\|_{\mathbb{U}} + \rho\varepsilon(\|\delta^k\|_{\mathbb{U}} + \|B\|\|r^k\|_{\mathbb{V}}) \\ &\leq (\|I - \rho B'B\| + \rho(\varepsilon^3 + 3\varepsilon^2 + 3\varepsilon)\|B\|^2)\|e_\varepsilon^k\|_{\mathbb{U}}. \end{aligned}$$

By the hypothesis of the Theorem, the constant $\|I - \rho B'B\| + \rho(\varepsilon^3 + 3\varepsilon^2 + 3\varepsilon)\|B\|^2$ is less than 1, which proves that $\{e_\varepsilon^k\}$ is a contraction.